Gravitational Waves from Extreme-Mass-Ratio Systems in Astrophysical Environments

Vitor Cardoso[1,2], Kyriakos Destounis,[3,4,5] Francisco Duque[2], Rodrigo Panosso Macedo[6], and Andrea Maselli[7,8]

[1]*Niels Bohr International Academy, Niels Bohr Institute, Blegdamsvej 17, 2100 Copenhagen, Denmark*
[2]*CENTRA, Departamento de Física, Instituto Superior Técnico–IST, Universidade de Lisboa–UL,*
Avenida Rovisco Pais 1, 1049 Lisboa, Portugal
[3]*Dipartimento di Fisica, Sapienza Università di Roma, Piazzale Aldo Moro 5, 00185, Roma, Italy*
[4]*INFN, Sezione di Roma, Piazzale Aldo Moro 2, 00185, Roma, Italy*
[5]*Theoretical Astrophysics, IAAT, University of Tübingen, 72076 Tübingen, Germany*
[6]*STAG Research Centre, University of Southampton, University Road SO17 1BJ, Southampton, United Kingdom*
[7]*Gran Sasso Science Institute (GSSI), I-67100 L'Aquila, Italy*
[8]*INFN, Laboratori Nazionali del Gran Sasso, I-67100 Assergi, Italy*

We establish a generic, fully relativistic formalism to study gravitational-wave emission by extreme-mass-ratio systems in spherically symmetric, nonvacuum black hole spacetimes. The potential applications to astrophysical setups range from black holes accreting baryonic matter to those within axionic clouds and dark matter environments, allowing one to assess the impact of the galactic potential, of accretion, gravitational drag, and halo feedback on the generation and propagation of gravitational waves. We apply our methods to a black hole within a halo of matter. We find fluid modes imparted to the gravitational-wave signal (a clear evidence of the black hole fundamental mode instability) and the tantalizing possibility to infer galactic properties from gravitational-wave measurements by sensitive, low-frequency detectors.

Introduction.—The birth of gravitational-wave (GW) astronomy ushered in a new era in gravitational physics and high-energy astrophysical phenomena [1,2]. GWs carry unique information about compact objects, most notably black hole (BH) systems, and grant us access to exquisite tests of the gravitational interaction in the strong field, highly dynamical regime [3–9].

They also bear precious information about the environment where compact binaries live [10–14]. This knowledge is important *per se*, and may inform us on how compact binaries are formed [15] or how BHs grow and evolve over cosmic times [16]. In addition, GWs are sensitive to accretion disk properties [17] and even on fundamental aspects, such as the existence of dark matter spikes in galactic centers [18–21]; on possibly new fundamental degrees of freedom that can condense around spinning BHs [22,23]; and finally on the nature and existence of BHs, as well as whether they are well described by the Kerr family, a quest which demands environmental effects to be disentangled from purely gravitational ones.

The above questions require a precise modeling of compact binaries in a fully relativistic setting. Unfortunately, the state of the art adopts at least one of the following approximations: a slow-motion quadrupole formula to estimate GW emission and the dynamics [24–27], Newtonian dynamical friction, or vacuum backgrounds. Recent attempts to refine the analysis by including some relativistic effects indicate that these can have a significant impact on

the conclusions one makes regarding detectability and parameter estimation [21,28,29].

Here—based on classical works on perturbation theory [30–37]—we develop a generic, fully relativistic formalism to handle environmental effects in extreme-mass-ratio inspirals (EMRIs) in spherically symmetric, but otherwise generic, backgrounds. These are inherently relativistic systems, expected to populate galactic centers and be observable with the upcoming space-based LISA mission [38–41], and for which Newtonian approximations are ill suited. Our framework is able to treat GW generation and propagation, but also includes matter perturbations and therefore is able to capture other environmental effects, such as dynamical friction [28,29], accretion, and halo feedback, and will be important to understand mode excitation or depletion of accretion disks, and even viscous heating in these systems. We use geometric units $G = c = 1$ everywhere.

Setup.—We wish to study a static, spherically symmetric spacetime describing a BH immersed in some environment, like an accretion disk or a dark matter halo, with line element

$$ds^2 = g^{(0)}_{\mu\nu} dx^\mu dx^\nu = -a(r)dt^2 + \frac{dr^2}{b(r)} + r^2 d\Omega^2, \quad (1)$$

where $d\Omega^2$ is the line element of the two-sphere, and characterized by a (anisotropic) stress tensor [42]

$$T_{\mu\nu}^{\text{env}(0)} = \rho u_\mu u_\nu + p_r k_\mu k_\nu + p_t \Pi_{\mu\nu}, \qquad (2)$$

where ρ is the total energy density of the fluid, p_r and p_t are its radial and tangential pressure respectively, u^μ the four velocity of the fluid, k^μ a unit spacelike vector orthogonal to u^μ, such that $k^\mu k_\mu = 1$ and $u^\mu k_\mu = 0$, and $\Pi_{\mu\nu} = g_{\mu\nu} + u_\mu u_\nu - k_\mu k_\nu$ is a projection operator orthogonal to u^μ and k^μ (environmental quantities are hereafter denoted with a superscript "env"). The functions $a(r)$ and $b(r)$ are to be determined by the physics; to prevent clustering throughout the text we drop the (t, r) dependence from all functions, unless necessary. We leave them general for most of the main body, but specialize to the physics of a supermassive BH surrounded by a halo of matter when necessary. The corresponding solution, which we will term galactic BHs (GBHs), was recently derived [43] and is characterized by the BH mass M_{BH}, halo mass M, and its spatial scale a_0 (see also Refs. [44,45] for generalizations and applications).

We now envision a secondary object of mass m_p (a star, asteroid, or stellar-mass BH for example) orbiting the above primary BH and causing perturbations to the geometry and matter stress tensor,

$$g_{\mu\nu} = g_{\mu\nu}^{(0)} + g_{\mu\nu}^{(1)}, \qquad T_{\mu\nu}^{\text{env}} = T_{\mu\nu}^{\text{env}(0)} + T_{\mu\nu}^{\text{env}(1)}, \quad (3)$$

where a superscript "(1)" denotes perturbations.

The spherical symmetry of the background allows for a separation of variables in the first-order quantities, expanding into tensor spherical harmonics, classified as *axial* and *polar*, according to their properties under parity [46–48]. In the Regge-Wheeler gauge [35,36,46–48], these are defined by radial functions $h_0^{\ell m}$, $h_1^{\ell m}$ (axial) and $K^{\ell m}$, $H_0^{\ell m}$, $H_1^{\ell m}$, $H_2^{\ell m}$ (polar), and a set of angular basis functions [35,36,49].

The perturbations induced by the orbiting object on the environment are known once its pressure, density, and velocity fluctuations are computed. These can also be expanded in harmonics. For example, a scalar quantity $X = p_t, p_r, \rho$ will have a perturbation $X^{(1)}$ expanded as

$$X^{(1)} = \sum_{\ell=2}^{\infty} \sum_{m=-\ell}^{\ell} \delta X^{\ell m}(t, r) Y^{\ell m}(\theta, \phi), \qquad (4)$$

with $Y^{\ell m}(\theta, \phi)$ being the standard spherical harmonics on the two-sphere. A similar procedure is applied to any vector quantity.

Finally, a barotropic equation of state provides a further relation between pressure, density variations, and the medium's speed of sound via

$$\delta p_{t,r}^{\ell m}(t, r) = c_{s_{t,r}}^2(r) \delta \rho^{\ell m}(t, r). \qquad (5)$$

Here, $c_{s_r}(r)$ and $c_{s_t}(r)$ are, respectively, the radial and transverse sound speeds. The explicit perturbed equations

are shown in the Supplemental Material [50] (see also Ref. [33] if $a = b$).

With the above procedure, perturbations to the environmental stress tensor are completely characterized. The source of these perturbations is modeled as a pointlike object with stress tensor

$$T_p^{\mu\nu} = m_p \int u_p^\mu u_p^\nu \frac{\delta^{(4)}(x^\mu - x_p^\mu(\tau))}{\sqrt{-g}} d\tau, \qquad (6)$$

where m_p is the mass of the secondary, τ its proper time, $x_p^\mu(\tau)$ its world line, and $u_p^\mu = dx_p^\mu/d\tau$ its four velocity. This stress-energy tensor can also be decomposed in terms of the angular basis [48,49], thereby separating the equations of motion. We will always assume that the pointlike secondary is on a geodesic of the background spacetime [Eq. (1)], and use this to simplify the equations of motion.

Evolution equations.—The perturbations are described by wave equations with a principal part expressed in terms of the operator $\mathcal{L}_v = v^2 \partial^2/\partial r_*^2 - \partial^2/\partial t^2$, with v the field's characteristic speed of propagation. Specifically, axial perturbations propagate with the speed of light $v = 1$ and are simply described in terms of a master variable $\chi = h_1^{\ell m} \sqrt{ab}/r$, governed by the equation

$$\mathcal{L}_1 \chi - V^{\text{ax}} \chi = S^{\text{ax}}, \qquad (7)$$

$$V^{\text{ax}} = \frac{a}{r^2}\left(\ell(\ell+1) - \frac{6m(r)}{r} + m'(r)\right), \qquad (8)$$

with $m(r) = r[1 - b(r)]/2$, the tortoise coordinate is defined by $dr_*/dr = \sqrt{ab}$, and the source term depends on the motion of the point particle (explicit expressions for circular motion are shown in the Supplemental Material [50]). The polar sector can be re-expressed as a system of three "wavelike" equations for $\vec{\phi} = (S, K, \delta\rho)$,

$$\hat{\mathcal{L}} \vec{\phi} = \hat{\mathbf{B}} \vec{\phi}_{,r^*} + \hat{\mathbf{A}} \vec{\phi} + \vec{S}_1, \qquad (9)$$

with $S = a/r(H_0 - K)$ and $\hat{\mathcal{L}} \vec{\phi} = (\mathcal{L}_1 \phi_1, \mathcal{L}_1 \phi_2, \mathcal{L}_{c_{s_r}} \phi_3)$, i.e., ϕ_1, ϕ_2 have characteristic velocity $v = 1$, and ϕ_3 has $v = c_{s_r}$.

We also study perturbations in the frequency domain by Fourier transforming the evolution equations. Instead of a second-order system for the polar sector, we worked instead with the first-order system

$$\frac{d\vec{\psi}}{dr} = \hat{\boldsymbol{\alpha}} \vec{\psi} + \vec{S}_2, \qquad (10)$$

with $\vec{\psi} = (H_1, H_0, K, W, \delta\rho)$, and W a fluid velocity quantity. The matrices $\hat{\mathbf{A}}$, $\hat{\mathbf{B}}$, $\hat{\boldsymbol{\alpha}}$, as well as source vectors $\vec{S}_i$ are shown in the Supplemental Material [50]. Particle

contributions enter as a source term $\vec{S}_1$, $\vec{S}_2$ for the metric variables.

We solve the above problem with two independent codes, based on different approaches, one in the time and the other in the frequency domain. Both use a smoothed distribution to approximate the point particle, $\sqrt{2\pi}\sigma\delta(r - r_p) = \exp(-(r - r_p)^2/(2\sigma^2))$ where the width σ is varied to assess numerical convergence. In the axial sector, the time domain code follows Refs. [51,52] which places the outer boundary condition at future null infinity by using the same hyperboloidal layers employed there. In the polar sector, the equations are solved in the usual radial tortoise cooordinate with physical boundaries placed sufficiently far, so that the physical quantities are extracted within the wave equation's causality domain and in a near vacuum region. For example, if we evolve the system for $t = 10^3 M_{\mathrm{BH}}$ and extract at $r_*^{\mathrm{ext}} = 500 M_{\mathrm{BH}}$, then the outer boundary should be placed further than $r_*^{\mathrm{out}} = 10^3 M_{\mathrm{BH}}$ to prevent any signal from being reflected back and affect the field values at the extraction radius. Unless stated otherwise, we use $r_*^{\mathrm{ext}} = \max\{10^2 a_0, 10^3 M_{\mathrm{BH}}\}$ as the extraction radius in the time domain code for the polar sector. The frequency domain code follows the framework from Ref. [53] in both sectors, with outer physical boundaries placed at $r^{\mathrm{ext}} = \max\{10^3/\Omega_p, 2a_0\}$, with Ω_p the orbital angular frequency. For the gravitational perturbations, we impose usual outgoing boundary conditions there and vanishing Dirichlet boundary conditions for the matter variables. The results from all codes agree within the numerical error when varying these parameters. Once the metric variables are computed, fluxes in GWs can be calculated. Our two codes are made freely available to the community [54,55].

Boundary conditions and sound speed.—Environments cause the presence of density waves that couple to gravity. To understand their asymptotic behavior, it is sufficient to examine a vacuum BH background of mass M_{BH}, to which the field equations reduce very far or very close to the horizon. For *constant* sound speeds, with the ansatz $\delta\rho = r^\alpha(r - 2M_{\mathrm{BH}})^\beta\Psi$, we find that Ψ is governed by the wave equation $\mathcal{L}_{c_{s_r}}\Psi - V\Psi = 0$ for

$$\alpha = \frac{1}{4}\left(-5 + \frac{1 + 4c_{s_t}^2}{c_{s_r}^2}\right), \qquad \beta = -\frac{3}{4} - \frac{1}{4c_{s_r}^2}, \qquad (11)$$

with $V = \mathcal{O}(r^{-2})$ at infinity and $V = [(1 - c_{s_r}^2)/(8c_{s_r}^2 M_{\mathrm{BH}})]^2$ at the horizon. The explicit form of V and wave equation for Ψ are identical to that obtained in Ref. [34] for isotropic fluids, with a suitable change of wave function H, once we identify $c_{s_r} = c_{s_t}$. Thus, close to the horizon density fluctuations propagate as an effectively massive scalar of mass $\mu_{\mathrm{eff}} = [(1 - c_{s_r}^2)/(8c_{s_r}^2 M_{\mathrm{BH}})]$. A rigorous analysis of the wave equation above is required to understand all the details of the density waves around BHs;
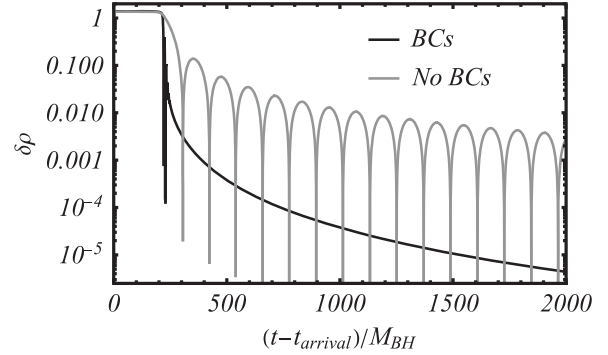

FIG. 1. Evolution of $\delta\rho$ in a Schwarzschild background with $c_{s_r} = 0.9$, $c_{s_t} = 0$ with different boundary conditions imposed. t_{arrival} corresponds to the time of arrival of the first direct signal. When $\delta\rho$ is left free at the horizon, an oscillatory tail sets in at late times, consistent with that of a scalar field of mass $\mu_{\mathrm{eff}}c_{s_r}$. Instead, when Dirichlet conditions are imposed at some cutoff radius r_{cut} (here $r_{\mathrm{cut}} = 3M_{\mathrm{BH}}$), we find a universal power-law decay independent of r_{cut} and c_{s_r}.

however, based on knowledge of massive fields around BHs [56–58], we expect an intermediate-time power-law tail of the form $\Psi \sim t^{-5/6}\sin(\mu_{\mathrm{eff}}c_{s_r})$, caused by back scattering in the near-horizon region and probably giving way to another power-law behavior dictated by the asymptotic region far from the BH [58]. Our numerical results in Fig. 1—for initial conditions $\delta\rho = 0$, $\partial_t\delta\rho = \exp[-(r_* - 100M_{\mathrm{BH}})^2/2]$, extracted at $r_* = 1000M_{\mathrm{BH}}$—support this claim. We find excellent agreement with an oscillatory term $\sin(\mu_{\mathrm{eff}}c_{s_r})$ and decay $t^{-5/6}$. We find a similar behavior for other values of c_{s_r}.

Configurations with a matter profile that vanishes at the horizon and spatial infinity have sound speeds expected to vanish asymptotically. For sound speed profiles that vanish as a power law at the boundaries, we find that regular density fluctuations $\delta\rho$ must satisfy Dirichlet conditions. We implement this restriction keeping c_{s_r} constant everywhere, but imposing Dirichlet conditions on fluid variables at some cutoff radius r_{cut} close to the BH. It is now possible to prove that the late time asymptotics is governed not by the near-horizon but by the large-r asymptotic behavior and that the field should decrease as t^{-3}, *independently of the multipole ℓ* [56]. This is seen clearly in our simulations in Fig. 1. The direct signal is followed by a universal power-law tail $\delta\rho \sim t^{-3}$, independently of cutoff radius r_{cut} and sound speed c_{s_r}.

Environment and spectral stability.—From now on, we always work with vanishing sound speeds at the boundaries. It is clear from the above that there are two characteristic speeds in the problem, the radial sound speed c_{s_r} and the light speed. Accordingly, and because the polar sector is coupled, we expect to have two families of perturbations, one led by gravity, traveling at the speed of light, and the other led by matter fluctuations, traveling at c_{s_r}. A clear
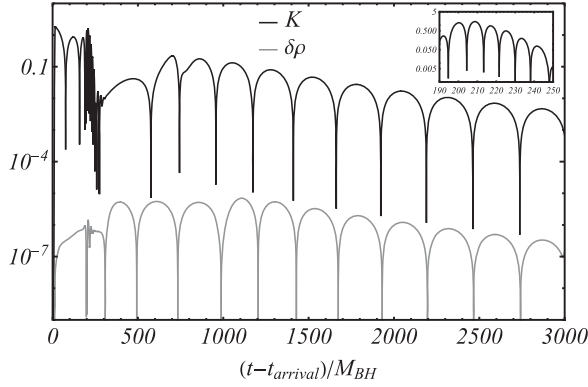
FIG. 2. Evolution of the metric and density perturbation K, $\delta\rho$, with $M = 10M_{\rm BH}$, $a_0 = 10M$. We impose Dirichlet conditions at $r_{\rm cut} = 3M_{\rm BH}$ and $c_{s_r} = [(2M_{\rm BH} + a_0)/(r + a_0)]^4$, so that it asymptotes to zero at large distances. At early times, BH ringdown is excited (inset for K); at late times, we observe a slowly decaying, fluid-driven mode with period $\propto a_0$. Notice a mutual conversion between GWs and density waves.

example of the importance of this coupling is seen through scattering a Gaussian wave packet of *gravitational* waves (initial conditions identical to those of Fig. 1, but for the metric function K). The metric perturbation K and $\delta\rho$ are shown in Fig. 2. We see conversion from GWs to density waves and vice versa, BH ringdown at early times, and a long-lived mode at late times. This is in essence a fluid mode, imprinted on the GW signal due to the coupling, and a clear example of spectral instability in BH quasinormal modes, which has attracted considerable interest recently [11,59–63], here seen in a realistic astrophysical setting.

Fluxes from orbiting particles.—We have tested our procedure and routines in the vacuum limit, i.e., using a GBH geometry [43] with low value of the halo mass $M = 10^{-6}M_{\rm BH}$, comparing the GW fluxes with those obtained by the Black Hole Perturbation Toolkit (BHPT) [64]. The results are summarized in Table I, and compare favorably both between different implementations with the BHPT tools in vacuum. It is clear from Table I that, for fixed BH mass, the fluxes are smaller in the presence of a halo. However, given that the binary sits at a nontrivial gravitational potential set by the halo, decreasing fluxes may amount to a redshift effect. We focus on realistic environments, where $M_{\rm BH} \ll M \ll a_0$. To linear order in M/a_0, $dr/dr_* \approx (1 - M/a_0)dr/dr_*^{\rm vac}$ where $r_*^{\rm vac}$ is the tortoise coordinate in a Schwarzschild geometry. Additionally, for compact EMRIs ($r_p \sim 10M_{\rm BH}$), $S^{\rm ax} \approx (1 - 3M/a_0)S_{\rm vac}^{\rm ax}$. Combining these, expanding Eq. (7) to linear order in M/a_0 one finds

$$\frac{d^2\psi^{\rm ax}}{d(r_*^{\rm vac})^2} + \left(\frac{\omega^2}{\gamma^2} - V_{\rm Schw}^{\rm ax}\right)\psi^{\rm ax} = \gamma S_{\rm Schw}^{\rm ax}, \qquad (12)$$

where $\gamma = 1 - M/a_0$ is a redshift factor. Thus, to linear order in γ the axial signal from a GBH is identical to that

TABLE I. Energy flux (in units of $m_p^2/M_{\rm BH}^2$) emitted to infinity in different modes by a particle in circular orbit around a GBH at radius $r_p = 7.9456M_{\rm BH}$. We show results for vacuum (first line of each mode) and for GBH with $c_{s_{r,t}} = (0.9, 0)$, $M = 10M_{\rm BH}$, and $a_0 = 10M$. $\dot{E}_\infty^t$ is computed with a time domain integrator, $\dot{E}_\infty^f$ in the frequency domain, and $\dot{E}_\infty^{\rm BHPT}$ corresponds to results from the BHPT, available only in vacuum. $\ell = m$ modes correspond to polar excitations whereas $\ell = m + 1$ correspond to axial ones.

ℓ	m	$\dot{E}_\infty^t$	$\dot{E}_\infty^f$	$\dot{E}_\infty^{\rm BHPT}$
2	1	8.1629×10^{-7}	8.1631×10^{-7}	8.1631×10^{-7}
		6.9156×10^{-7}	6.9158×10^{-7}	
2	2	1.7068×10^{-4}	1.7062×10^{-4}	1.7062×10^{-4}
		1.6077×10^{-4}	1.6208×10^{-4}	
3	2	2.5198×10^{-7}	2.5199×10^{-7}	2.5198×10^{-7}
		2.1611×10^{-7}	2.1612×10^{-7}	
3	3	2.5490×10^{-5}	2.5473×10^{-5}	2.5471×10^{-5}
		2.3163×10^{-5}	2.3140×10^{-5}	
4	3	5.7750×10^{-8}	5.7749×10^{-8}	5.7749×10^{-8}
		5.0252×10^{-8}	5.0252×10^{-8}	
4	4	4.7352×10^{-6}	4.7260×10^{-6}	4.7253×10^{-6}
		4.0458×10^{-6}	4.0823×10^{-6}	

from a Schwarzschild BH, with redshifted frequency and mass; in other words, the two setups are equivalent with the identification

$$(\Omega_p^{\rm vac}, \omega^{\rm vac}, m_p^{\rm vac}) \to \left(\frac{\Omega_p}{\gamma}, \frac{\omega}{\gamma}, \gamma m_p\right). \qquad (13)$$

Axial perturbations do not couple to matter perturbations, and a simple propagation redshift seems adequate. The polar sector is more involved, and requires numerical study.

In Fig. 3, we present numerical results that confirm this picture, showing fluxes as a function of the frequency of the GWs being measured by a distant stationary observer. For axial modes ($\ell = 2$, $m = 1$), the differences between a vacuum and nonvacuum environment are seemingly large, but as can be seen in Fig. 3, fluxes from a GBH are indeed well described by redshifted fluxes in vacuum. The agreement is all the better for larger halo mass M, smaller compactness M/a_0. For galactic configurations, it leads to relative differences that are extremely small.

Note that for small scales, $a_0\omega \lesssim 1$, the radiation wavelength is larger than the halo itself, and redshift is suppressed. At large frequencies redshifted vacuum fluxes are an excellent description of our results, for axial perturbations. Indeed, we also find that quasinormal modes conform to such a description since they are high-frequency phenomena in this setup [65].

Polar fluctuations are coupled to the fluid, as we saw, and a naive redshift is not sufficient to describe GW generation and propagation. Figure 3 shows one of our exciting
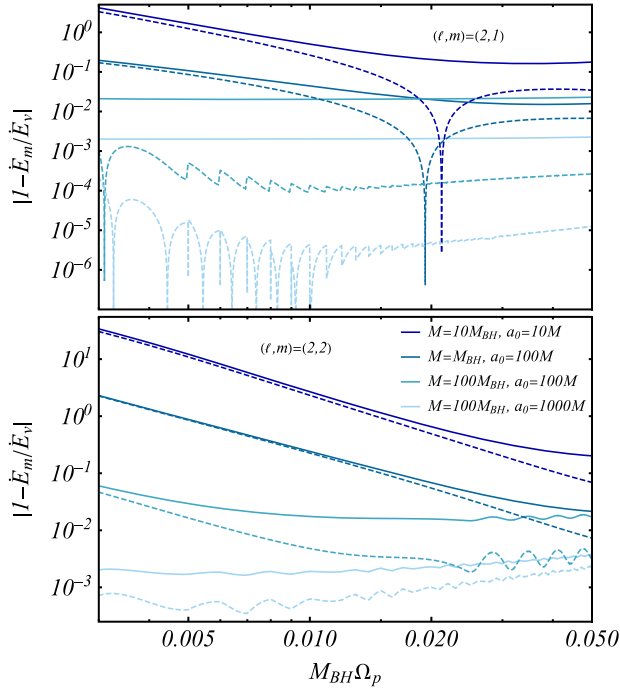
FIG. 3. Top panel: relative difference between the energy flux of the $\ell = 2$, $m = 1$ mode emitted by the EMRI for different GBH configurations ($\dot{E}_m$) and in vacuum ($\dot{E}_v$), as a function of GW frequency (solid lines). Frequency range corresponds to a secondary location $r_p = 50M_{\rm BH}$ down to $r_p = 6M_{\rm BH}$. Dashed lines show the vacuum result redshifted according to Eq. (13). Bottom panel: same as the top panel but for the $\ell = m = 2$ mode.

findings: polar perturbations are less prone to redshift effects, even in regions of parameter space corresponding to large, near-galactic scales. Thus, together with the axial sector they are able to break possible degeneracies, with sensitive, low-frequency detectors.

Independently of that, our results clearly indicate the ability of GW astronomy to strongly constrain smaller scale matter distributions around BHs. At $\omega M_{\rm BH} = 0.02$, the relative flux difference between a vacuum and a GBH with $M = 0.1M_{\rm BH}$ and $a_0 = 10^2 M, 10^3 M$ is $\sim 10\%, 1\%$ respectively. These numbers are within reach of next generation detectors [66]. Compare with GRAVITY's constraints on the environment of the Sgr A* star [67], but note that GW astronomy allows similar constraints for a large number of sources.

Discussion.—Our Letter serves as a proof-of-concept for the ability to study environmental effects in GW physics at a full relativistic level. A natural next step is to apply it to other environments, for example by taking input from recent GRMHD simulations of accretion [12,68], or to add rotation to the BH.

The application of our relativistic framework to galactic EMRIs immersed in a halo shows that environments can easily destabilize the BH spectra, as had recently been suggested with toy models [11,60–63]; it is unknown at this

point if environmental resonances can be excited by supermassive BHs, long before merger; however, our results show how the coupling to the environment changes GW generation and propagation.

Nonetheless, there are important issues that remain to be answered. The energy flux emitted in GWs contains contributions directly from the binding energy of the binary but also from the environment. It is unclear if energy balance arguments alone are sufficient to evolve such systems, even in an adiabatic approach, or if self-force methods [69] are necessary, and whether they too need to be modified to take environments fully into account. This aspect is of particular relevance if the binary is able to resonantly excite the proper modes of the environment. In addition to energy carried by GWs, there will also be viscous heating, which can be included in the formalism. We plan to address some of these problems in future work.

[1] B. P. Abbott *et al.* (LIGO Scientific and Virgo Collaborations), Observation of Gravitational Waves from a Binary Black Hole Merger, Phys. Rev. Lett. **116,** 061102 (2016).

[2] B. P. Abbott *et al.* (LIGO-Virgo Collaborations), GWTC-1: A Gravitational-Wave Transient Catalog of Compact Binary Mergers Observed by LIGO and Virgo during the First and Second Observing Runs, Phys. Rev. X **9**, 031040 (2019).

[3] K. Yagi and L. C. Stein, Black hole based tests of general relativity, Classical Quantum Gravity **33**, 054001 (2016).

[4] L. Barack *et al.*, Black holes, gravitational waves and fundamental physics: A roadmap, Classical Quantum Gravity **36**, 143001 (2019).

[5] V. Cardoso and P. Pani, Testing the nature of dark compact objects: A status report, Living Rev. Relativity **22**, 4 (2019).

[6] V. Baibhav *et al.*, Probing the nature of black holes: Deep in the mHz gravitational-wave sky, Exp. Astron. **51**, 1385 (2021).

[7] R. Abbott *et al.* (LIGO Scientific, VIRGO, and KAGRA Collaborations), Tests of General Relativity with GWTC-3, arXiv:2112.06861.

[8] M. H.-Y. Cheung *et al.*, Nonlinear effects in black hole ringdown, arXiv:2208.07374.

[9] K. Mitman *et al.*, Nonlinearities in black hole ringdowns, arXiv:2208.07380.

[10] N. Yunes, B. Kocsis, A. Loeb, and Z. Haiman, Imprint of Accretion Disk-Induced Migration on Gravitational Waves from Extreme Mass Ratio Inspirals, Phys. Rev. Lett. **107**, 171103 (2011).

[11] E. Barausse, V. Cardoso, and P. Pani, Can environmental effects spoil precision gravitational-wave astrophysics?, Phys. Rev. D **89**, 104059 (2014).

[12] A. Derdzinski, D. D'Orazio, P. Duffell, Z. Haiman, and A. MacFadyen, Evolution of gas disc–embedded intermediate mass ratio inspirals in the *LISA* band, Mon. Not. R. Astron. Soc. **501**, 3540 (2021).

[13] V. Cardoso, C. F. B. Macedo, and R. Vicente, Eccentricity evolution of compact binaries and applications to gravitational-wave physics, Phys. Rev. D **103**, 023015 (2021).

[14] L. Zwick, P. R. Capelo, and L. Mayer, Priorities in gravitational waveform modelling for future space-borne detectors: Vacuum accuracy or environment?, arXiv:2209.04060.

[15] Z. Pan, Z. Lyu, and H. Yang, Wet extreme mass ratio inspirals may be more common for spaceborne gravitational wave detection, Phys. Rev. D **104**, 063007 (2021).

[16] V. Cardoso, T. Ikeda, R. Vicente, and M. Zilhão, Parasitic black holes: The swallowing of a fuzzy dark matter soliton, arXiv:2207.09469.

[17] L. Speri, A. Antonelli, L. Sberna, S. Babak, E. Barausse, J. R. Gair, and M. L. Katz, Measuring accretion-disk effects with gravitational waves from extreme mass ratio inspirals, arXiv:2207.10086.

[18] K. Eda, Y. Itoh, S. Kuroyanagi, and J. Silk, New Probe of Dark-Matter Properties: Gravitational Waves from an Intermediate-Mass Black Hole Embedded in a Dark-Matter Minispike, Phys. Rev. Lett. **110**, 221101 (2013).

[19] C. F. B. Macedo, P. Pani, V. Cardoso, and L. C. B. Crispino, Into the lair: Gravitational-wave signatures of dark matter, Astrophys. J. **774**, 48 (2013).

[20] B. J. Kavanagh, D. A. Nichols, G. Bertone, and D. Gaggero, Detecting dark matter around black holes with gravitational waves: Effects of dark-matter dynamics on the gravitational waveform, Phys. Rev. D **102**, 083006 (2020).

[21] N. Speeney, A. Antonelli, V. Baibhav, and E. Berti, Impact of relativistic corrections on the detectability of dark-matter spikes with gravitational waves, Phys. Rev. D **106**, 044027 (2022).

[22] R. Brito, V. Cardoso, and P. Pani, Superradiance: New frontiers in black hole physics, Lect. Notes Phys. **906**, 1 (2015).

[23] A. Maselli, N. Franchini, L. Gualtieri, T. P. Sotiriou, S. Barsanti, and P. Pani, Detecting fundamental fields with LISA observations of gravitational waves from extreme mass-ratio inspirals, Nat. Astron. **6**, 464 (2022).

[24] S. Babak, H. Fang, J. R. Gair, K. Glampedakis, and S. A. Hughes, 'Kludge' gravitational waveforms for a test-body orbiting a Kerr black hole, Phys. Rev. D **75**, 024005 (2007); **77**, 049902 (2008).

[25] K. Destounis, A. G. Suvorov, and K. D. Kokkotas, Testing spacetime symmetry through gravitational waves from extreme-mass-ratio inspirals, Phys. Rev. D **102**, 064041 (2020).

[26] K. Destounis, A. G. Suvorov, and K. D. Kokkotas, Gravitational-Wave Glitches in Chaotic Extreme-Mass-Ratio Inspirals, Phys. Rev. Lett. **126**, 141102 (2021).

[27] K. Destounis and K. D. Kokkotas, Gravitational-wave glitches: Resonant islands and frequency jumps in non-integrable extreme-mass-ratio inspirals, Phys. Rev. D **104**, 064023 (2021).

[28] R. Vicente and V. Cardoso, Dynamical friction of black holes in ultralight dark matter, Phys. Rev. D **105**, 083008 (2022).

[29] D. Traykova, K. Clough, T. Helfer, E. Berti, P. G. Ferreira, and L. Hui, Dynamical friction from scalar dark matter in the relativistic regime, Phys. Rev. D **104**, 103014 (2021).

[30] K. S. Thorne and A. Campolattaro, Non-radial pulsation of general-relativistic stellar models. I. Analytic analysis for L >= 2, Astrophys. J. **149**, 591 (1967).

[31] S. L. Detweiler and L. Lindblom, On the nonradial pulsations of general relativistic stellar models, Astrophys. J. **292**, 12 (1985).

[32] S. Chandrasekhar and V. Ferrari, On the non-radial oscillations of a star, Proc. R. Soc. A **432**, 247 (1991).

[33] Y. Kojima, Equations governing the nonradial oscillations of a slowly rotating relativistic star, Phys. Rev. D **46**, 4289 (1992).

[34] G. Allen, N. Andersson, K. D. Kokkotas, and B. F. Schutz, Gravitational waves from pulsating stars: Evolving the perturbation equations for a relativistic star, Phys. Rev. D **58**, 124012 (1998).

[35] O. Sarbach and M. Tiglio, Gauge invariant perturbations of Schwarzschild black holes in horizon penetrating coordinates, Phys. Rev. D **64**, 084016 (2001).

[36] K. Martel and E. Poisson, Gravitational perturbations of the Schwarzschild spacetime: A practical covariant and gauge-invariant formalism, Phys. Rev. D **71**, 104003 (2005).

[37] K. Martel, Gravitational wave forms from a point particle orbiting a Schwarzschild black hole, Phys. Rev. D **69**, 044025 (2004).

[38] J. R. Gair, S. Babak, A. Sesana, P. Amaro-Seoane, E. Barausse, C. P. L. Berry, E. Berti, and C. Sopuerta, Prospects for observing extreme-mass-ratio inspirals with LISA, J. Phys. Conf. Ser. **840**, 012021 (2017).

[39] Z. Pan and H. Yang, Formation rate of extreme mass ratio inspirals in active galactic nuclei, Phys. Rev. D **103**, 103018 (2021).

[40] P. Amaro-Seoane *et al.*, Astrophysics with the laser interferometer space antenna, arXiv:2203.06016.

[41] K. G. Arun *et al.* (LISA Collaboration), New horizons for fundamental physics with LISA, Living Rev. Relativity **25**, 4 (2022).

[42] G. Raposo, P. Pani, M. Bezares, C. Palenzuela, and V. Cardoso, Anisotropic stars as ultracompact objects in General Relativity, Phys. Rev. D **99**, 104072 (2019).

[43] V. Cardoso, K. Destounis, F. Duque, R. P. Macedo, and A. Maselli, Black holes in galaxies: Environmental impact on gravitational-wave generation and propagation, Phys. Rev. D **105**, L061501 (2022).

[44] R. A. Konoplya and A. Zhidenko, Solutions of the Einstein equations for a black hole surrounded by a galactic halo, Astrophys. J. **933**, 166 (2022).

[45] K. Destounis, A. Kulathingal, K. D. Kokkotas, and G. O. Papadopoulos, Gravitational-wave imprints of compact and galactic-scale environments in extreme-mass-ratio binaries, arXiv:2210.09357.

[46] T. Regge and J. A. Wheeler, Stability of a Schwarzschild singularity, Phys. Rev. **108**, 1063 (1957).

[47] F. J. Zerilli, Effective Potential for Even Parity Regge-Wheeler Gravitational Perturbation Equations, Phys. Rev. Lett. **24**, 737 (1970).

[48] F. J. Zerilli, Gravitational field of a particle falling in a schwarzschild geometry analyzed in tensor harmonics, Phys. Rev. D **2**, 2141 (1970).

[49] N. Sago, H. Nakano, and M. Sasaki, Gauge problem in the gravitational selfforce. 1. Harmonic gauge approach in the Schwarzschild background, Phys. Rev. D **67**, 104017 (2003).

[50] See Supplemental Material at http://link.aps.org/supplemental/10.1103/PhysRevLett.129.241103 for technical details on the formalism adopted in the manuscript, the explicit form of the set of equations for the matter and metric perturbations, as well as the mathematical procedure used to integrate them.

[51] A. Zenginoglu and G. Khanna, Null Infinity Waveforms from Extreme-Mass-Ratio Inspirals in Kerr Spacetime, Phys. Rev. X **1**, 021017 (2011).

[52] P. A. Sundararajan, G. Khanna, and S. A. Hughes, Towards adiabatic waveforms for inspiral into Kerr black holes. I. A new model of the source for the time domain perturbation equation, Phys. Rev. D **76**, 104005 (2007).

[53] V. Cardoso, C. F. B. Macedo, P. Pani, and V. Ferrari, Black holes and gravitational waves in models of minicharged

dark matter, J. Cosmol. Astropart. Phys. 05 (2016) 054; 04 (2020) E01.

[54] grit repo, https://centra.tecnico.ulisboa.pt/network/grit/files/.

[55] sgrep repo, https://github.com/masellia/SGREP/.

[56] E. S. C. Ching, P. T. Leung, W. M. Suen, and K. Young, Wave propagation in gravitational systems: Late time behavior, Phys. Rev. D **52**, 2118 (1995).

[57] S. Hod and T. Piran, Late time tails in gravitational collapse of a selfinteracting (massive) scalar field and decay of a selfinteracting scalar hair, Phys. Rev. D **58**, 044018 (1998).

[58] H. Koyama and A. Tomimatsu, Asymptotic tails of massive scalar fields in Schwarzschild background, Phys. Rev. D **64**, 044014 (2001).

[59] J. L. Jaramillo, R. P. Macedo, and L. Al Sheikh, Pseudospectrum and Black Hole Quasinormal Mode Instability, Phys. Rev. X **11**, 031003 (2021).

[60] J. L. Jaramillo, R. P. Macedo, and L. A. Sheikh, Gravitational Wave Signatures of Black Hole Quasinormal Mode Instability, Phys. Rev. Lett. **128**, 211102 (2022).

[61] K. Destounis, R. P. Macedo, E. Berti, V. Cardoso, and J. L. Jaramillo, Pseudospectrum of Reissner-Nordström black holes: Quasinormal mode instability and universality, Phys. Rev. D **104**, 084091 (2021).

[62] M. H.-Y. Cheung, K. Destounis, R. P. Macedo, E. Berti, and V. Cardoso, Destabilizing the Fundamental Mode of Black Holes: The Elephant and the Flea, Phys. Rev. Lett. **128**, 111103 (2022).

[63] E. Berti, V. Cardoso, M. H.-Y. Cheung, F. Di Filippo, F. Duque, P. Martens, and S. Mukohyama, Stability of the fundamental quasinormal mode in time-domain observations against small perturbations, Phys. Rev. D **106**, 084011 (2022).

[64] Black Hole Perturbation Toolkit, http://bhptoolkit.org/.

[65] V. Cardoso *et al.*, Environmental effects in gravitational generation and emission: perturbations of black holes in astrophysical environments (to be published).

[66] B. Bonga, H. Yang, and S. A. Hughes, Tidal Resonance in Extreme Mass-Ratio Inspirals, Phys. Rev. Lett. **123**, 101103 (2019).

[67] R. Abuter *et al.* (GRAVITY Collaboration), Mass distribution in the Galactic Center based on interferometric astrometry of multiple stellar orbits, Astron. Astrophys. **657**, L12 (2022).

[68] L. Zwick, A. Derdzinski, M. Garg, P. R. Capelo, and L. Mayer, Dirty waveforms: multiband harmonic content of gas-embedded gravitational wave sources, Mon. Not. R. Astron. Soc. **511**, 6143 (2022).

[69] L. Barack and A. Pound, Self-force and radiation reaction in general relativity, Rep. Prog. Phys. **82**, 016904 (2019).